

The Effects of Ca²⁺ Binding on the Dynamic Properties of a Designed Ca²⁺-Binding Protein^{†,‡}

Wei Yang, Anna L. Wilkins, Shunyi Li, Yiming Ye, and Jenny J. Yang*

Department of Chemistry, Center for Drug Design, Georgia State University, Atlanta, Georgia 30303

Received March 13, 2005; Revised Manuscript Received April 13, 2005

ABSTRACT: The effects of Ca²⁺ binding on the dynamic properties of Ca²⁺-binding proteins are important in Ca²⁺ signaling. To understand the role of Ca²⁺ binding, we have successfully designed a Ca²⁺-binding site in the domain 1 of rat CD2 (denoted as Ca.CD2) with the desired structure and retained function. In this study, the backbone dynamic properties of Ca.CD2 have been investigated using ¹⁵N spin relaxation NMR spectroscopy to reveal the effect of Ca²⁺ binding on the global and local dynamic properties without the complications of multiple interactive Ca²⁺ binding and global conformational change. Like rat CD2 (rCD2) and human CD2 (hCD2), residues involved in the recognition of the target molecule CD48 exhibit high flexibility. Mutations N15D and N17D that introduce the Ca²⁺ ligands increase the flexibility of the neighboring residues. Ca²⁺-induced local dynamic changes occur mainly at the residues proximate to the Ca²⁺-binding pocket or the residues in loop regions. The β -strand B of Ca.CD2 that provides two Asp for the Ca²⁺ undergoes an *S*² decrease upon the Ca²⁺ binding, while the DE-loop that provides one Asn and one Asp undergoes an *S*² increase. Our study suggests that Ca²⁺ binding has a differential effect on the rigidity of the residues depending on their flexibility and location within the secondary structure.

As a second messenger, Ca²⁺ regulates many biological processes through interactions with Ca²⁺-binding proteins located in various cellular environments (1, 2). The effects of Ca²⁺ binding on the dynamic properties of proteins have been shown to be important in Ca²⁺ signaling and protein functions. The dynamic effects of Ca²⁺ binding have been investigated using EF-hand proteins, in which multiple EF-hand motifs are often paired within one domain. The binding of Ca²⁺ to calbindin D_{9k}, troponin C, and calmodulin (3–8) results in a more rigid local conformation and an overall entropy loss in the EF-loops. The Ca²⁺-binding sites in EF-pairs are structurally and energetically coupled (4, 6, 8, 9), and Ca²⁺ binding induces changes in the conformational flexibility and dynamic properties at the remote structure regions (6, 8, 10). Extracellular proteins such as cadherins, Ca²⁺-dependent EGF-like¹ modules, and low-density lipoprotein receptors have multiple clustered Ca²⁺-binding sites with affinities corresponding to the extracellular Ca²⁺ concentration. Ca²⁺ binding results in changes of local conformation and dynamic properties that are essential for the function and stability of these proteins (11–15). The study of their Ca²⁺ binding effect is more challenging due to their tendency to oligomerize and the exchange between Ca²⁺-free and Ca²⁺-bound populations. Clearly, Ca²⁺ binding has different consequences on the flexibility and thermodynamics of proteins with different affinities.

To understand the role of Ca²⁺ binding in the dynamic and functional properties of the protein and the key factors contributing to Ca²⁺ binding, our lab has established a design approach to introduce a single Ca²⁺-binding site into a functional host protein. This design approach is particularly advantageous since the effect of Ca²⁺ binding can be clearly revealed without the complications of multiple interactive Ca²⁺ binding and global conformational change. We have chosen the domain 1 of rat CD2 as the host protein in order to elucidate the effect of Ca²⁺ upon dynamic properties and molecular recognition. CD2 was the first protein revealed to be important in promoting intercellular adhesion and signal transduction (16) by interacting with the partner molecules CD48 (in rat) or CD58 (in human) (17–20). It is one of the best-characterized cell adhesion molecules in the immunoglobulin superfamily with a topology similar to the Ca²⁺-dependent cell adhesion molecules cadherins (17, 21, 22). Nine β -strands are sandwiched in two layers of GFCC'C'' and BED strands (23–25). It has served as a model system to understand the mechanism of molecular recognition and to establish a correlation among the structure, dynamics, and function of macromolecules (26, 27). The backbone dynamic properties of both rat and human CD2 have been investigated previously. It has been found that the surface related to the target molecule binding possesses high flexibility (26, 27).

We have successfully designed a Ca²⁺-binding site into the domain 1 of rat CD2 (denoted Ca.CD2) (28) by taking into account the key geometric and chemical properties of the Ca²⁺ sites without splicing in an entire, known metal-binding domain (30–32). It is the first stable, rationally designed Ca²⁺-binding protein (33, 34). The Ca²⁺ site is formed by two discontinuous sections of the polypeptide (Figure 1). It requires two mutations (N15D and N17D) at β -strand B and utilizes existing side-chain oxygen atoms

[†] This work is supported in part by the NSF MCB-0092486 and NIH GM 62999-1 grants to J.J.Y.

[‡] The NMR assignment of Ca.CD2 has been deposited in the BioMagResBank under accession number 6201.

* To whom correspondence should be addressed. Fax, 404-651-2751; phone, 404-651-4620; e-mail, chejyy@panther.gsu.edu.

¹ Abbreviations: CD2, cluster of differentiation 2; hCD2, human CD2; rCD2, rat CD2; EGF, epidermal growth factor; NOE, nuclear Overhauser effect; NMR, nuclear magnetic resonance.

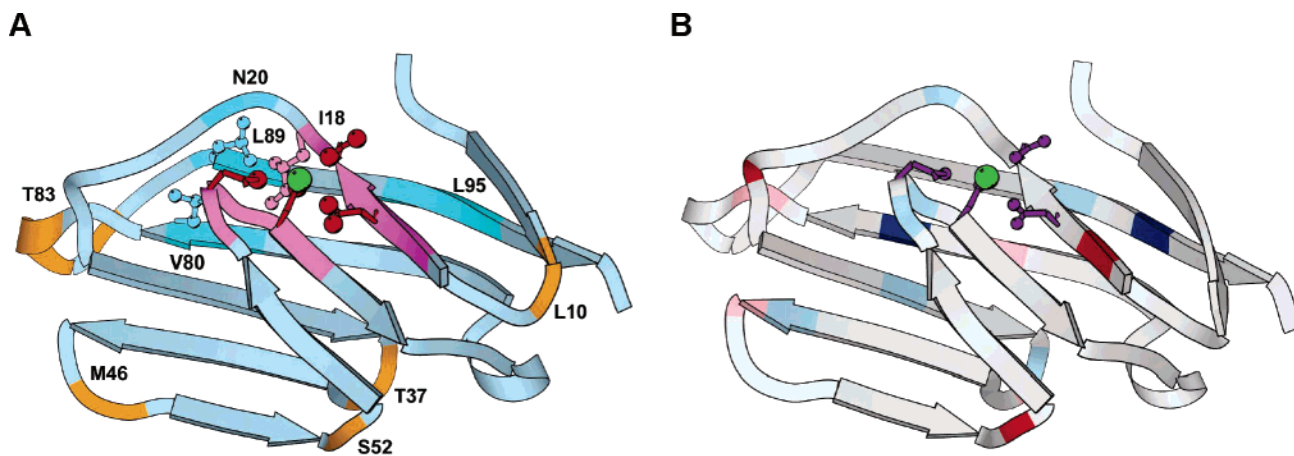


FIGURE 1: (A) The structure of Ca.CD2 (1T6W) with the bound Ca^{2+} (green ball) is shown (28). The side chains of the Ca^{2+} ligands are shown in red. The Ca^{2+} -binding residues and the adjacent residues are shown in violet. The residues close to strand B are represented in cyan. The loops that undergo relatively large dynamic property changes are shown in orange. Only one residue is labeled when continuous residues are colored. The figure is prepared using Molscript (29). (B) The entropy changes of Ca.CD2 induced by Ca^{2+} are represented. The residues with entropy gains of more than 1 kJ/mol are labeled pink, and those with more than 2 kJ/mol are labeled red. The residues with entropy losses of more than 1 kJ/mol are labeled light blue, and those with more than 2 kJ/mol are labeled blue.

(N60 and D62) at the DE-loop as Ca^{2+} ligands. Direct interference with the molecular recognition of CD2 is avoided since the designed site is located on the opposite surface of the protein. As a result, Ca.CD2 retains the binding ability to CD48. The Ca^{2+} binding results in a small but significant decrease in the CD48-binding affinity compared to the Ca^{2+} -free form. Ca.CD2 has a Ca^{2+} affinity of 1.4 mM (K_d), which is similar to that of extracellular Ca^{2+} -binding proteins. The binding of Ca^{2+} only induced local conformational changes in Ca.CD2 (28).

In this study, we report our investigation of the Ca^{2+} effect on the backbone dynamic properties of Ca.CD2 using ^{15}N spin relaxation NMR spectroscopy. It provides insight into the effect of Ca^{2+} binding on the global and local dynamic properties of a weak Ca^{2+} -binding protein with K_d at mM range without the complications of multiple interactive Ca^{2+} binding and global conformational change. The dynamic parameters have been measured and derived in the absence and presence of Ca^{2+} . The results show that, like rCD2 and hCD2, residues of Ca.CD2 involved in the recognition of CD48 exhibit high flexibility. Residues in the Ca^{2+} -binding pocket, the neighboring residues, and the loop residues exhibit relatively large Ca^{2+} -induced dynamic changes. Our study shows that Ca^{2+} binding has differential effects on the rigidity of the residues in Ca.CD2 depending on their location within the secondary structure. The change of conformational entropy upon Ca^{2+} binding has also been discussed.

MATERIALS AND METHODS

Protein Expression and Purification. The Ca.CD2 protein was engineered, expressed, and purified as previously described (28).

Relaxation Time and NOE Measurement. The assignment of NMR spectra of Ca.CD2 at 25 °C is achieved through standard methods and procedures as previously described (28). Because several additional peaks can be observed at low temperatures without large spectral differences, the dynamic studies were performed at 4 °C on a 500 MHz magnet. The new assignments at 4 °C were achieved by taking advantage of several spectra collected between 4 and 25 °C. The T_1 and T_2 relaxation times were measured using

conventional pulse sequences (35) except that a sinc one-lobe selective pulse is used to put water back along the z -axis (36). The center frequency of ^1H is put on water (4.76 ppm) and that of ^{15}N is put on the amide region (119.5 ppm). The spectral widths were 6600 Hz with 2048 complex data points in the ^1H dimension and 1800 Hz with 128 increments in the ^{15}N dimension. The arrayed relaxation times for the T_1 measurements are 0.1, 0.2, 0.3, 0.4, 0.5, 0.6, 0.8, 1.0, 1.2, 1.5, and 3.0 s. A 180° ^1H pulse is used every 5 ms during the relaxation time to eliminate the effects of cross-correlation between ^1H - ^{15}N dipolar coupling and chemical shift anisotropy relaxation (37, 38). The arrayed relaxation times for the T_2 measurements are from 10 to 210 ms with a step of 20 ms. A 180° ^{15}N pulse is used every 625 μs , and a 180° ^1H pulse is used every 10 ms during the relaxation time (37, 38). The ^{15}N -enriched proteins (0.3 mM) are in 20 mM PIPES at pH 6.8 with 10 mM CaCl_2 or 1 mM EGTA. The apparent relaxation times were obtained by fitting the intensity decays with a single-exponential function. The measurement of NOE effects was performed using the gNnoe pulse sequence in the VARIAN Protein-Pack (38). The samples and the other experimental conditions were the same as for the T_1 and T_2 measurements. The saturation time for the NOE spectra was 4 s, and the relaxation delay was set to 4 s for the control spectra (NONOE spectra). ^1H saturation is achieved by the application of 120° pulses every 5 ms before the first ^{15}N pulse (38). Each 1D increment is an average of 128 scans to enhance the signal/noise ratio. The height and volume of each peak were obtained by performing the INTEGRATE function in the SPARKY program (Godard & Kneller at University of California). The NOE factors for each resonance were the ratio of peak volume of the NOE and NONOE spectra. The uncertainties of the NOE factors were estimated to be less than 10% based on the analysis of signal/noise ratios and the comparison between the Ca^{2+} -loaded and Ca^{2+} -free forms, which are adequate for the following dynamic analysis. First, the signal/noise ratios given by the SPARKY program are above 30 for most of the resonances. For example, only eight residues in the NOE spectrum of the EGTA form possess signal/noise ratios less than 30. Three of them (S3, T89, and N90) have signal/noise

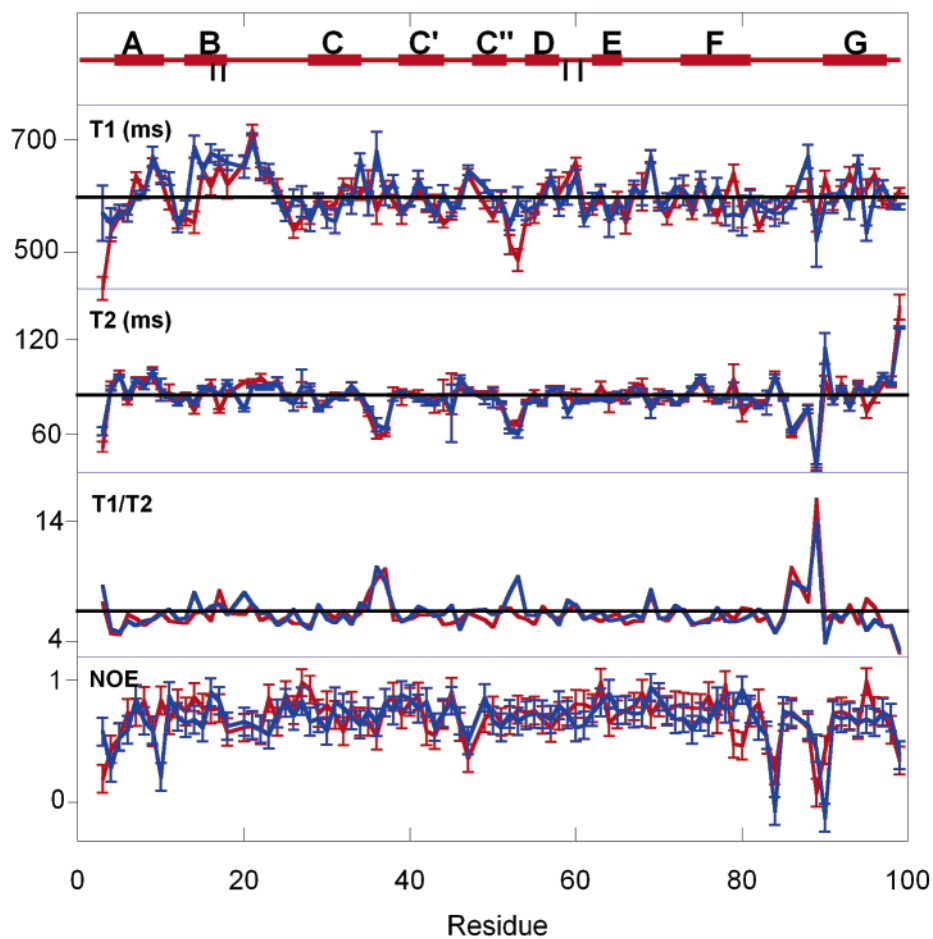


FIGURE 2: From top to bottom, the secondary structure, T_1 , T_2 , T_1/T_2 ratio, and NOE of Ca.CD2 in the absence (red) and presence (blue) of Ca²⁺ at 4 °C are shown with error bars of T_1 and T_2 . The lines in the diagrams represent the value of 600 ms, 90 ms and 6.667, respectively. The positions of the Ca²⁺ ligands are marked using perpendicular lines.

ratios less than 20. Second, the similarity of NOE patterns between Ca²⁺-free and Ca²⁺-loaded forms indicates the accuracy of the measurement. More than 60% (59 in 94) of the residues have net differences less than 0.1 between the two forms.

Model-Free Calculation. The S^2 order parameters of Ca.CD2 were calculated using Modelfree version 4.15 provided by Dr. Palmer at Columbia University (39, 40). Apparent R_1 , R_2 , and NOE together with the NMR structure of Ca.CD2 (1T6W) were input to simulate the S^2 by optimizing the axially symmetric diffusion model using Brent's implementation of Powell's method for multidimensional minimization. The internuclear ¹H-¹⁵N distance r_{NH} is assumed to be 1.02 Å, and the ¹⁵N chemical shift anisotropy (CSA) tensor is assumed to be -172 ppm (41). The model selection for each spin followed the flowchart that was suggested by Mandel et al. (39, 40). The majority of the spins were simulated by S^2 only (model 1), except for the following: residues N20, F21, Q22, M46, K47, T83, N84, and N90 in both forms; A9, I18, F42, K43, T79, V80, and L98 in Ca²⁺-free form; and L10, M23, A59, G74, and Y76 in Ca²⁺-loaded form were simulated by S^2 and τ_c together (model 2). T37, S52, G53, T69, and L95 in both forms, D17 in Ca²⁺-free form, and I14, S36, and L58 in Ca²⁺-loaded form were simulated by S^2 and R_{ex} together (model 3). S3, G4, T5, T86, and I88 in both forms, and G35 and S36 in Ca²⁺-free form were simulated by S^2 , τ_c , and R_{ex} together (model 4). No model fit well for residues L89 and

E99 based on the criteria suggested by Mandel et al. Model 4 was used in the final calculation, since it gives smaller fitting errors than model 5 does (40, 42). The $D_{||}/D_{\perp}$ and τ_m were also obtained from the calculation, and the axes of inertia were automatically assigned by the Modelfree program.

The entropy differences between the Ca²⁺-free and Ca²⁺-loaded forms are derived from the S^2 values from the equation given by Yang and Kay (43). Since the classical description of conformational entropy breaks down when S^2 is over 0.95, the entropy changes of the residues (I14, S52, and G53) with S^2 greater than 0.95 are calculated assuming their S^2 values are 0.95 (6, 43).

RESULTS AND DISCUSSIONS

Dynamic Parameters of Ca.CD2. The longitudinal relaxation time (T_1), transverse relaxation time (T_2), T_1/T_2 ratios, and NOE of Ca²⁺-free (solid line) and Ca²⁺-bound (dashed line) forms of Ca.CD2 are shown in Figure 2. All dynamic investigations were carried out at 4 °C to observe additional signals, including G53 and S36 at the loop regions. These residues cannot be observed at 25 °C possibly due to the existence of intermediate exchange processes. The backbone dynamic parameters were measured for all residues except R1, D2, P19, P48, and R87. The averaged T_1 values are 596 and 604 ms and the averaged T_2 values are 89.2 and 89.0 ms for Ca²⁺-free and Ca²⁺-loaded Ca.CD2, respectively.

Table 1: Summary of the Dynamic Properties of Ca·CD2

parameter	1 mM EGTA	10 mM Ca ²⁺
T_1	596 ms	604 ms
T_2	89.2 ms	89.0 ms
NOE	0.736	0.726
T_1/T_2	6.82	6.92
S^2	0.846	0.846
τ_m	9.05 ns	9.20 ns
D_{\parallel}/D_{\perp}	0.873	0.869

Most T_1 values have less than 100 ms deviations from the average except for some residues at the N-terminal, BC-loop, and C'D-loop. Only a few residues in the loop regions have obviously short T_2 values. Correspondingly, the average T_1/T_2 ratios are 6.82 and 6.92 for the EGTA and Ca²⁺ forms, respectively (Table 1). Residues with obviously large T_1/T_2 ratios (at CC'- and FG-loop) are those with short T_2 relaxation times. The average NOE values of Ca·CD2 are 0.736 and 0.726 for the EGTA and Ca²⁺ forms, respectively. The small NOE factors, which are frequently associated with slow internal motions (9), are mainly observed at the FG-loop.

The general order parameter S^2 , chemical exchange rate (R_{ex}), and effective correlation time (τ_e) of Ca·CD2 were derived from the apparent R_1 , R_2 , and NOE of each residue together with the NMR structure (1T6W) (28) using the Modelfree 4.15 program (39, 40). The simulated isotropic rotational correlation time (τ_m) for the global diffusion tensor is 9.05 and 9.20 ns, and the D_{\parallel}/D_{\perp} ratio is 0.873 and 0.869 in the Ca²⁺-free and the Ca²⁺-bound forms, respectively (Table 1).

The average S^2 values of Ca·CD2 are approximately 0.846 in both forms (Table 1), which are in accordance with values reported for rCD2 (27) and other highly ordered proteins (44). Most of the residues with higher S^2 values are at structured regions (Figure 3). However, it is noteworthy that several loop residues that connect two layers of Ca·CD2 but are located close to the GFCC'C'' layer, including S52 and G53 at the C'D-loop, residues 25–28 at the BC-loop, and S73 and G74 at the EF-loop, possess above average S^2 values. S52 and G53 retain the highest S^2 values in the absence of Ca²⁺. The rigidity at this position is also observed in hCD2 (45). The high rigidity of these residues is likely to play an important role in maintaining the tertiary structure of CD2 and its variants (24, 46).

Most of the flexible residues ($S^2 < 0.8$) are located at the loop regions, of which the FG-loop not only retains the lowest S^2 values but also possesses high R_{ex} and slow τ_e . For example, L89 has a τ_e slower than 600 ps and an R_{ex} higher than 15 Hz. This suggests that the FG-loop undergoes active dynamic processes, such as local conformational change. The results agree well with the relatively low-resonance intensity of residues 87–89 in the $\{^{15}\text{N}, ^1\text{H}\}$ -HSQC spectra, specifically L89, which possesses the lowest intensity of all the assigned residues.

Comparison of Ca·CD2 and CD2. The overall dynamic properties of Ca·CD2 are similar to hCD2 and rCD2. The average S^2 of Ca·CD2 (0.846) is slightly higher than the reported value (0.81) for rCD2. The trend of the S^2 distribution along the peptide sequence in CD2 (17, 27, 45, 47, 48) is maintained in Ca·CD2. The isotropic rotational correlation times of 9.05 and 9.20 ns for Ca·CD2 are close to that of 9.5 ns for glycosylated hCD2, which agree well

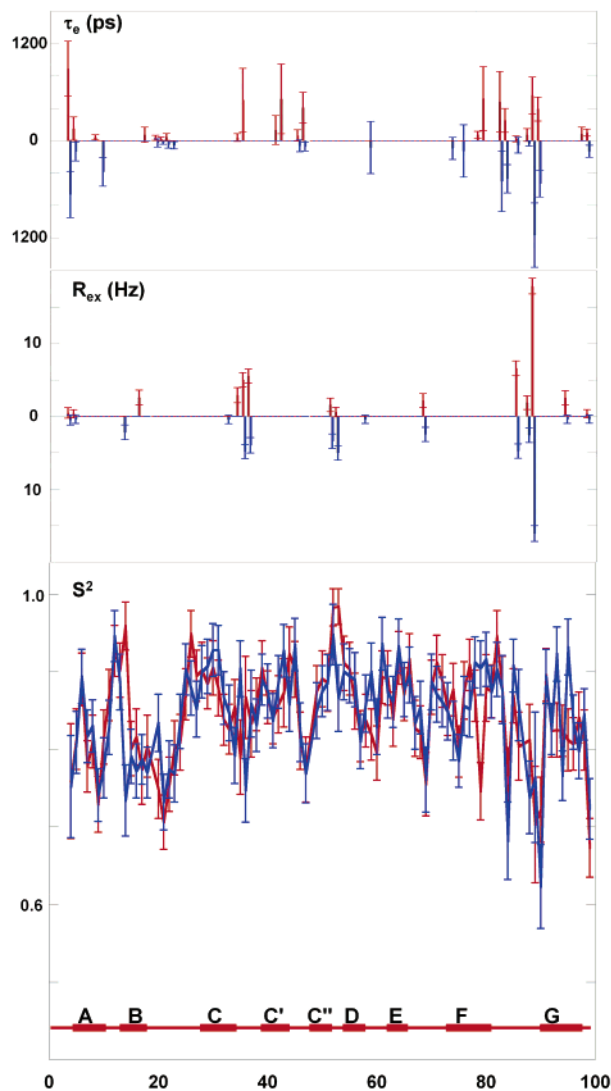


FIGURE 3: Secondary structure, S^2 , R_{ex} , and τ_e (from bottom to top) of Ca·CD2 in the absence (red) and presence (blue) of Ca²⁺.

with other proteins of similar size (45). In addition, as in hCD2 and rCD2 (17, 27, 45, 47, 48), most of the residues with low S^2 , high R_{ex} , and/or slow τ_e in Ca·CD2 are located at the CD48-binding surface (Figures 1 and 3), such as T37, L38, and T86. The flexibility of this surface may facilitate the binding by improving the interactions of residues to their partner residues on the target molecule and by allowing the protein to adjust its local conformation for the complex repacking, because (at least) a local conformation change is always expected for optimal molecular recognition.

There are several dynamic differences between Ca·CD2 and rCD2 despite the overall similarity. First, strand B (D15 to I18) that holds the two mutations has a decreased S^2 . In addition, the proximately located FG-loop, in which V80 and L89 are less than 4 Å from I18, has the most dramatic S^2 decrease accompanied by high R_{ex} and slow τ_e . In rCD2, T79 possesses high R_{ex} at high-protein concentrations, while the residues at the N-terminal of the FG-loop possess R_{ex} values between 1 and 4 Hz (47). In Ca·CD2, the R_{ex} of L89 is greater than 15 Hz and that of T86 also exceeds 5 Hz, while T79 has no detectable chemical exchange. This difference is likely induced by the mutations instead of Ca²⁺

binding because it has been observed in both forms of Ca.CD2.

Classification of the Residues Affected by Ca²⁺ Binding. Ca.CD2 provides a model to reveal the dynamic effect of Ca²⁺ binding on the global and local environment of weak Ca²⁺-binding, extracellular proteins. Given the weak binding ($K_d \sim 0.1\text{--}3\text{ mM}$) and the environmental Ca²⁺ concentration (1–10 mM), the extracellular Ca²⁺ proteins are usually partially bounded. For example, the μs – ms time scale motions have been observed in loaded fibrillin-1 cbEGF12–13 and cbEGF32–33 (14). At the experimental conditions, Ca.CD2 is also not fully saturated ($\sim 87\%$ of protein are Ca²⁺-loaded given the K_d of 1.4 mM and total 10 mM Ca²⁺ in solution). The attempt to saturate the protein with high-salt concentration may introduce nonspecific binding and is impractical. The existence of a Ca²⁺-free population in the presence of Ca²⁺ reduces the observed S^2 difference between the two forms. Therefore, the Ca²⁺-induced change discussed here is semiquantitative. Nevertheless, neither the trends nor the relative values of different residues is likely to be altered. In Ca.CD2, it is unlikely that the existence of different populations significantly alters the S^2 measurement since the observed R_{ex} and T_2 at the Ca²⁺-binding pocket undergo only minor changes with the addition of Ca²⁺ (Figures 2 and 3).

Ca²⁺ binding does not change the overall dynamic properties of Ca.CD2. The average T_1 , T_2 , NOE, S^2 order parameter, D_{\parallel}/D_{\perp} ratio, and overall diffusion correlation time are similar in the presence of EGTA or Ca²⁺ (Table 1). Only several residues exhibit larger dynamic property changes over the experimental uncertainty (Figures 2–4). Because of the large uncertainty of simulation and the existence of exchange between the two forms at the experimental conditions, the τ_c and R_{ex} changes are not conclusive and will not be further analyzed here. Eight residues have an S^2 difference greater than 0.1 upon Ca²⁺ binding. They are I14, S36, G53, and N90 with lowered rigidity and G35, T79, L93, and L95 with enhanced rigidity. I14 undergoes the largest S^2 decrease from 0.96 to 0.73.

The residues with large dynamic changes upon Ca²⁺ binding can be classified into three groups according to their locations. The first group contains the Ca²⁺ ligands and the adjacent residues, which are sequences of I14 to I18 and A59 to L63. It is noteworthy that the adjacent residues have greater dynamic changes than the ligand residues themselves. For example, upon Ca²⁺ binding, at strand B, I14 becomes significantly dynamic with the greatest T_1 elongation, T_1/T_2 ratio increase, and S^2 decrease. On the other hand, A59 at the DE-loop becomes more rigid with the largest T_2 decrease and S^2 increase (Figures 2–4). In addition, Ca²⁺ binding provides differential effects on strand B and the DE-loop, each of which provides two residues for Ca²⁺ binding. Strand B becomes more flexible while the DE-loop becomes more rigid upon Ca²⁺ binding. Furthermore, the residues at strand B undergo greater changes than those at the DE-loop (Figures 2–4). These different effects are likely due to the B-strand providing two negatively charged residues to the positively charged Ca²⁺ instead of one from the DE-loop. Therefore, the electrostatic forces introduced by Ca²⁺ binding are more significant on strand B. The difference between the loop and the β -strand structures may also contribute to the different effects.

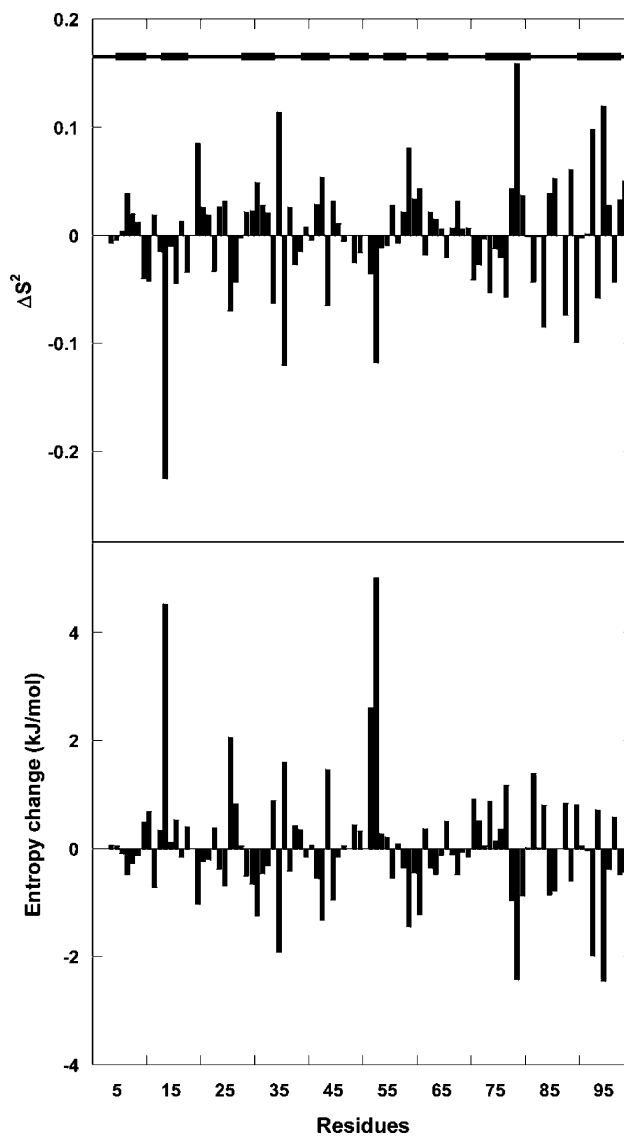


FIGURE 4: S^2 order parameters and entropy change of Ca.CD2. Positive values represent the S^2 increase and entropy decrease in the presence of Ca²⁺. The bars at the top represent the β -strand of the protein.

The second group contains the residues proximate to the Ca²⁺-binding pocket, specifically strand B, including N20 at the BC-loop, V80 and L89 at the FG-loop, and L93 and L95 at strand G (Figure 1). These residues are less than 5 Å from one of the residues 16–18 at strand B. The adjacent residues T79, N90, and D94 can be classified into this group. The Ca²⁺-induced changes in this group are likely due to their direct interaction with strand B. Since strands F and G and the FG-loop are involved in target-molecule recognition, the decrease in CD48-binding affinity for the Ca²⁺-loaded form of Ca.CD2 (28) is likely a result of the dynamic changes in this group.

The third group contains the residues at the flexible regions of Ca.CD2 far from the Ca²⁺-binding pocket, such as S36, T37, S52, and G53 (Figure 1). With either increased or decreased flexibility, these loop regions buffered the indirect effects on the protein caused by Ca²⁺ binding. Correspondingly, no other β -strand residues except those at β -strands B, F, and G undergo backbone dynamic changes greater than the average values for any dynamic parameters measured.

Comparison of Ca.CD2 to Other Ca²⁺-Binding Proteins. The effects of the Ca²⁺ binding on dynamic properties have been investigated using the EF-hand proteins. By assuming that bond amide ¹⁵N-¹H vector motions are approximated by the diffusion-in-a-cone model, the conformational entropy can be semiquantitatively calculated from *S*² values of ligand-free and -loaded forms (49, 50). The binding of Ca²⁺ to calbindin D_{9k}, troponin C, and calmodulin often leads to a more rigid local conformation and a loss of entropy in the EF-loops (3–8). Such local *S*² increase and entropy loss is not observed in Ca.CD2. In contrast, the total *S*² value of residues at the Ca²⁺-binding pocket (I14 to I18 and A59 to L63) is slightly decreased by 0.138. Hence, the net conformational entropy change (+1.87 kJ/mol) around the Ca²⁺-binding pocket is energetically favorable, or at least not unfavorable, for Ca²⁺ binding. I14 contributes greatly to the entropy gain (+4.06 kJ/mol), which is partially from the conformation exchange between two forms. When model 1 was used for all residues (which means the contributions of slow motion and chemical exchange are not included in the calculation), the *S*² of I14 with Ca²⁺ increases from 0.73 to 0.81 while the overall *S*² decrease of the Ca²⁺-binding pocket is 0.199. Correspondingly, the entropy gain of the pocket is increased to 4.23 kJ/mol although the contribution from I14 decreased to 3.15 kJ/mol. The results suggest that the trend of Ca²⁺ effect observed in Ca.CD2 is not altered by the conformational change between apo and loaded forms. The similar entropy gains upon ligand bindings have been observed for several proteins such as the mouse major urinary protein MUP-I or RIIα (10, 51–55). In addition, the small local entropy gain observed in Ca.CD2 is similar to the binding of the second Ca²⁺ to calbindin D_{9k} (8, 10). Although there is a large entropy loss in the initial Ca²⁺ binding, the paired EF-loops in calbindin D_{9k} exhibit a small net entropy gain upon binding the second Ca²⁺. A large entropy decrease in the initial binding steps was needed to destabilize the intermediate states and to favor the second Ca²⁺ binding process.

In summary, in Ca.CD2, residues that are involved in the recognition of the target molecule CD48 exhibit high flexibility similar to that of rCD2 and hCD2. The binding of Ca²⁺ does not change the overall structure and dynamic properties of Ca.CD2. It mainly affects the local dynamic properties of three groups: the Ca²⁺-binding ligands, the nearby residues, and the loop residues with different magnitudes. The β-strand B and the surrounding residues have greater dynamic changes than the DE-loop. Ca²⁺ binding results in an increase in the *S*² at the DE-loop and a decrease at strand B. This differential effect is likely a result of the charge as well as the secondary structure differences. Ca²⁺ binding may increase the rigidity of the flexible loops and exhibit less pronounced effects at a well-defined structural region. Unlike EF-hand proteins, no entropy loss upon Ca²⁺ binding was observed around the Ca²⁺-binding pocket in Ca.CD2. This study provides us with insight into the differences between the strong and weak Ca²⁺-binding proteins.

ACKNOWLEDGMENT

The authors wish to thank Dan Adams, James Prestegard, Thomas Weldeghiorghis, Hsiau-wei Lee, and other members in Dr. Yang's lab for critical review and helpful discussion.

The authors also wish to thank T. D. Goddard and D. G. Kneller at the University of California for providing the SPARKY program.

SUPPORTING INFORMATION AVAILABLE

HSQC spectra of Ca.CD2 at 25 and 4 °C, the tables of dynamic properties in the absence and presence of Ca²⁺. This material is available free of charge via the Internet at <http://pubs.acs.org>.

REFERENCES

- Berridge, M. J., Bootman, M. D., and Lipp, P. (1998) Calcium—a life and death signal, *Nature* 395, 645–648.
- Glusker, J. P. (1991) Structural aspects of metal liganding to functional groups in proteins, *Adv. Protein Chem.* 42, 1–76.
- Kordel, J., Skelton, N. J., Akke, M., Palmer, A. G., III, and Chazin, W. J. (1992) Backbone dynamics of calcium-loaded calbindin D_{9k} studied by two-dimensional proton-detected ¹⁵N NMR spectroscopy, *Biochemistry* 31, 4856–4866.
- Akke, M., Skelton, N. J., Kordel, J., Palmer, A. G., III, and Chazin, W. J. (1993) Effects of ion binding on the backbone dynamics of calbindin D_{9k} determined by ¹⁵N NMR relaxation, *Biochemistry* 32, 9832–9844.
- Lee, A. L., Kinnear, S. A., and Wand, A. J. (2000) Redistribution and loss of side chain entropy upon formation of a calmodulin-peptide complex, *Nat. Struct. Biol.* 7, 72–77.
- Spyracopoulos, L., Gagne, S. M., Li, M. X., and Sykes, B. D. (1998) Dynamics and thermodynamics of the regulatory domain of human cardiac troponin C in the apo- and calcium-saturated states, *Biochemistry* 37, 18032–18044.
- Tjandra, N., Kuboniwa, H., Ren, H., and Bax, A. (1995) Rotational dynamics of calcium-free calmodulin studied by ¹⁵N NMR relaxation measurements, *Eur. J. Biochem.* 230, 1014–1024.
- Maler, L., Blankenship, J., Rance, M., and Chazin, W. J. (2000) Site–site communication in the EF-hand Ca²⁺-binding protein calbindin D_{9k}, *Nat. Struct. Biol.* 7, 245–250.
- Gagne, S. M., Tsuda, S., Spyracopoulos, L., Kay, L. E., and Sykes, B. D. (1998) Backbone and methyl dynamics of the regulatory domain of troponin C: anisotropic rotational diffusion and contribution of conformational entropy to calcium affinity, *J. Mol. Biol.* 278, 667–686.
- Stone, M. J. (2001) NMR relaxation studies of the role of conformational entropy in protein stability and ligand binding, *Acc. Chem. Res.* 34, 379–388.
- Muranyi, A., Evenas, J., Stenberg, Y., Stenflo, J., and Drakenberg, T. (2000) Characterization of the EGF-like module pair 3–4 from vitamin K-dependent protein S using NMR spectroscopy reveals dynamics on three separate time scales and extensive effects from calcium binding, *Biochemistry* 39, 15742–15756.
- Kurniawan, N. D., O'Leary, J. M., Thamlitz, A. M., Sofair, R., Werner, J. M., Stenflo, J., and Downing, A. K. (2004) N-Terminal domain linkage modulates the folding properties of protein S epidermal growth factor-like modules, *Biochemistry* 43, 9352–9360.
- Kurniawan, N. D., Aliabadizadeh, K., Brereton, I. M., Kroon, P. A., and Smith, R. (2001) NMR structure and backbone dynamics of a concatemer of epidermal growth factor homology modules of the human low-density lipoprotein receptor, *J. Mol. Biol.* 311, 341–356.
- Smallridge, R. S., Whiteman, P., Werner, J. M., Campbell, I. D., Handford, P. A., and Downing, A. K. (2003) Solution structure and dynamics of a calcium binding epidermal growth factor-like domain pair from the neonatal region of human fibrillin-1, *J. Biol. Chem.* 278, 12199–12206.
- Werner, J. M., Knott, V., Handford, P. A., Campbell, I. D., and Downing, A. K. (2000) Backbone dynamics of a cbEGF domain pair in the presence of calcium, *J. Mol. Biol.* 296, 1065–1078.
- Hunig, T. (1985) The cell surface molecule recognized by the erythrocyte receptor of T lymphocytes. Identification and partial characterization using a monoclonal antibody, *J. Exp. Med.* 162, 890–901.
- McAlister, M. S., Mott, H. R., van der Merwe, P. A., Campbell, I. D., Davis, S. J., and Driscoll, P. C. (1996) NMR analysis of interacting soluble forms of the cell–cell recognition molecules CD2 and CD48, *Biochemistry* 35, 5982–5991.

18. Davis, S. J., and van der Merwe, P. A. (1996) The structure and ligand interactions of CD2: implications for T-cell function, *Immunol. Today* 17, 177–187.
19. Dustin, M. L., Ferguson, L. M., Chan, P. Y., Springer, T. A., and Golan, D. E. (1996) Visualization of CD2 interaction with LFA-3 and determination of the two-dimensional dissociation constant for adhesion receptors in a contact area, *J. Cell Biol.* 132, 465–474.
20. Rudd, P. M., Wormald, M. R., Stanfield, R. L., Huang, M., Mattsson, N., Speir, J. A., DiGennaro, J. A., Fetrow, J. S., Dwek, R. A., and Wilson, I. A. (1999) Roles for glycosylation of cell surface receptors involved in cellular immune recognition, *J. Mol. Biol.* 293, 351–366.
21. Nagar, B., Overduin, M., Ikura, M., and Rini, J. M. (1996) Structural basis of calcium-induced E-cadherin rigidification and dimerization, *Nature* 380, 360–364.
22. Driscoll, P. C., Cyster, J. G., Campbell, I. D., and Williams, A. F. (1991) Structure of domain I of rat T lymphocyte CD2 antigen, *Nature* 353, 762–765.
23. Wilkins, A. L., Yang, W., and Yang, J. J. (2003) Structural biology of the cell adhesion protein CD2: from molecular recognition to protein folding and design, *Curr. Protein Pept. Sci.* 4, 367–373.
24. Yang, J. J., Ye, Y., Carroll, A., Yang, W., and Lee, H. W. (2001) Structural biology of the cell adhesion protein CD2: alternatively folded states and structure–function relation, *Curr. Protein Pept. Sci.* 2, 1–17.
25. van der Merwe, P. A., McNamee, P. N., Davies, E. A., Barclay, A. N., and Davis, S. J. (1995) Topology of the CD2-CD48 cell-adhesion molecule complex: implications for antigen recognition by T cells, *Curr. Biol.* 5, 74–84.
26. Kitao, A., and Wagner, G. (2000) A space-time structure determination of human CD2 reveals the CD58-binding mode, *Proc. Natl. Acad. Sci. U.S.A.* 97, 2064–2068.
27. Chen, H. A., Pfuhl, M., and Driscoll, P. C. (2002) The pH dependence of CD2 domain I self-association and ¹⁵N chemical exchange broadening is correlated with the anomalous pK_a of Glu41, *Biochemistry* 41, 14680–14688.
28. Yang, W., Wilkins, A. L., Ye, Y., Liu, Z. R., Li, S. Y., Urbauer, J. L., Hellinga, H. W., Kearney, A., van der Merwe, P. A., and Yang, J. J. (2005) Design of a calcium-binding protein with desired structure in a cell adhesion molecule, *J. Am. Chem. Soc.* 127, 2085–2093.
29. Kraulis, P. J. (1991) MOLSCRIPT: a program to produce both detailed and schematic plots of protein structures, *J. Appl. Crystallogr.* 24, 946–950.
30. Pardon, E., Haezebrouck, P., De Baetselier, A., Hooke, S. D., Fancourt, K. T., Desmet, J., Dobson, C. M., Van Dael, H., and Joniau, M. (1995) A Ca(2+)-binding chimera of human lysozyme and bovine alpha-lactalbumin that can form a molten globule, *J. Biol. Chem.* 270, 10514–10524.
31. Joniau, M., Haezebrouck, P., Noyelle, K., and Van Dael, H. (2001) Structural basis for the appearance of a molten globule state in chimeric molecules derived from lysozyme and alpha-lactalbumin, *Proteins* 44, 1–11.
32. Kuroki, R., and Yutani, K. (1998) Structural and thermodynamic responses of mutations at a Ca²⁺ binding site engineered into human lysozyme, *J. Biol. Chem.* 273, 34310–34315.
33. Yang, W., Jones, L. M., Isley, L., Ye, Y., Lee, H. W., Wilkins, A., Liu, Z. R., Hellinga, H. W., Malchow, R., Ghazi, M., and Yang, J. J. (2003) Rational design of a calcium-binding protein, *J. Am. Chem. Soc.* 125, 6165–6171.
34. Wilkins, A. L., Ye, Y., Yang, W., Lee, H. W., Liu, Z. R., and Yang, J. J. (2002) Metal-binding studies for a de novo designed calcium-binding protein, *Protein Eng.* 15, 571–574.
35. Kay, L. E., Keifer, P., and Saarinen, T. (1992) Pure absorption gradient enhanced heteronuclear single quantum correlation spectroscopy with improved sensitivity, *J. Am. Chem. Soc.* 114, 10663–10665.
36. Bendall, M. R. (1995) Heteronuclear *J*-coupling precession during spin-lock and adiabatic pulses—use of adiabatic inversion pulses in high-resolution NMR, *J. Magn. Reson., Ser. A* 116, 46–58.
37. Kay, L. E., Nicholson, L. K., Delaglio, F., Bax, A., and Torchia, D. A. (1992) Pulse sequences for removal of the effects of cross-correlation between dipolar and chemical-shift anisotropy relaxation mechanism on the measurement of heteronuclear T1 and T2 values in proteins, *J. Magn. Reson.* 97, 359–375.
38. Farrow, N. A., Muhandiram, R., Singer, A. U., Pascal, S. M., Kay, C. M., Gish, G., Shoelson, S. E., Pawson, T., Forman-Kay, J. D., and Kay, L. E. (1994) Backbone dynamics of a free and phosphopeptide-complexed Src homology 2 domain studied by ¹⁵N NMR relaxation, *Biochemistry* 33, 5984–6003.
39. Palmer, A. G., III, Rance, M., and Wright, P. E. (1991) Intramolecular motions of a zinc finger DNA-binding domain from Xfin characterized by proton-detected natural abundance ¹³C heteronuclear NMR spectroscopy, *J. Am. Chem. Soc.* 113, 4371–4380.
40. Mandel, A. M., Akke, M., and Palmer, A. G., 3rd. (1995) Backbone dynamics of *Escherichia coli* ribonuclease HI: correlations with structure and function in an active enzyme, *J. Mol. Biol.* 246, 144–163.
41. Palmer, A. G., III (2001) NMR probes of molecular dynamics: overview and comparison with other techniques, *Annu. Rev. Biophys. Biomol. Struct.* 30, 129–155.
42. Chen, J., Brooks, C. L., III, and Wright, P. E. (2004) Model-free analysis of protein dynamics: assessment of accuracy and model selection protocols based on molecular dynamics simulation, *J. Biomol. NMR* 29, 243–257.
43. Yang, D., and Kay, L. E. (1996) Contributions to conformational entropy arising from bond vector fluctuations measured from NMR-derived order parameters: application to protein folding, *J. Mol. Biol.* 263, 369–382.
44. Goodman, J. L., Pagel, M. D., and Stone, M. J. (2000) Relationships between protein structure and dynamics from a database of NMR-derived backbone order parameters, *J. Mol. Biol.* 295, 963–978.
45. Wyss, D. F., Dayie, K. T., and Wagner, G. (1997) The counter-receptor binding site of human CD2 exhibits an extended surface patch with multiple conformations fluctuating with millisecond to microsecond motions, *Protein Sci.* 6, 534–542.
46. Yang, J. J., Carroll, A. R., Yang, W., Ye, Y., and Nguyen, C. N. (2000) Nonnative intermediate state of acid-stable beta-sheet protein, *Cell Biochem. Biophys.* 33, 253–273.
47. Pfuhl, M., Chen, H. A., Kristensen, S. M., and Driscoll, P. C. (1999) NMR exchange broadening arising from specific low affinity protein self-association: analysis of nitrogen-15 nuclear relaxation for rat CD2 domain I, *J. Biomol. NMR* 14, 307–320.
48. Wyss, D. F., Choi, J. S., Li, J., Knoppers, M. H., Willis, K. J., Arulanandam, A. R., Smolyar, A., Reinherz, E. L., and Wagner, G. (1995) Conformation and function of the N-linked glycan in the adhesion domain of human CD2, *Science* 269, 1273–1278.
49. Akke, M., Bruschweiler, R., and Palmer, A. G. (1993) NMR order parameters and free-energy—an analytical approach and its application to cooperative Ca²⁺ binding by Calbindin-D(9k), *J. Am. Chem. Soc.* 115, 9832–9833.
50. Li, Z., Raychaudhuri, S., and Wand, A. J. (1996) Insights into the local residual entropy of proteins provided by NMR relaxation, *Protein Sci.* 5, 2647–2650.
51. Fushman, D., Weisemann, R., Thuring, H., and Ruterjans, H. (1994) Backbone dynamics of ribonuclease-T1 and its complex with 2'gmp studied by 2-dimensional heteronuclear NMR-spectroscopy, *J. Biomol. NMR* 4, 61–78.
52. Stivers, J. T., Abeygunawardana, C., and Mildvan, A. S. (1996) ¹⁵N NMR relaxation studies of free and inhibitor-bound 4-oxalocrotonate tautomerase: backbone dynamics and entropy changes of an enzyme upon inhibitor binding, *Biochemistry* 35, 16036–16047.
53. Yuan, P., Marshall, V. P., Petzold, G. L., Poorman, R. A., and Stockman, B. J. (1999) Dynamics of stromelysin/inhibitor interactions studied by N-15 NMR relaxation measurements: comparison of ligand binding to the S-1-S-3 and S-1'-S-3' subsites, *J. Biomol. NMR* 15, 55–64.
54. Zidek, L., Novotny, M. V., and Stone, M. J. (1999) Increased protein backbone conformational entropy upon hydrophobic ligand binding, *Nat. Struct. Biol.* 6, 1118–11121.
55. Fayos, R., Melacini, G., Newlon, M. G., Burns, L., Scott, J. D., and Jennings, P. A. (2003) Induction of flexibility through protein–protein interactions, *J. Biol. Chem.* 278, 18581–18587.

BI050463N